Fabrication and phase modulation in organic single-crystalline configurationally locked, phenolic polyene OH1 waveguides

Christoph Hunziker, Seong-Ji Kwon, Harry Figi, Mojca Jazbinsek, Peter Günter

Institute of Quantum Electronics, Nonlinear Optics Laboratory, ETH Zurich, CH-8093 Zurich, Switzerland

nlo@phys.ethz.ch

Abstract: A novel and promising technique for the fabrication of electro-optically active single crystalline organic waveguides from 2-{3-(4-hydroxystyryl)-5,5-dimethylcyclohex-2-enylidene}malononitrile (OH1) is presented. OH1 is an interesting material for photonic applications due to the large electro-optic coefficients ($r_{333} = 109 \pm 4$ pm/V at 632.8 nm) combined with a relatively high crystal symmetry (orthorhombic with point group *mm*2). Due to the very favorable growth characteristics, large-area (> 150 mm^2) single crystalline thin films with very good optical quality and thickness between $0.05 - 10$ μm have been grown on amorphous glass substrates. We have developed and optimized optical lithography and reactive ion etching processes for the fabrication of wire optical waveguides with dimensions of $w \times h = 3.4 \times 3.5$ μm^2 and above. The technique is capable of producing low loss integrated optical waveguides having propagation losses of 2 dB/cm with a high refractive index contrast between core-cladding and core-substrate of $\Delta n = 1.23$ and 0.72, respectively at 980 nm. Electro-optic phase modulation in these waveguides has been demonstrated at 632.8 nm and 852 nm. Calculations show that with an optimized electrode configuration the half-wave voltage $\times$ length product $V_\pi \cdot L$ can be reduced from 8.4 Vcm, as obtained in our device, to 0.3 Vcm in the optimized case. This allows for the fabrication of sub-1 V half-wave voltage, organic electro-optic modulators with highly stable chromophore orientation.

OCIS codes: (160.2100) Electro-optical materials; (230.2090) Electro-optical devices; (130.4110) Modulators.

References and links

1. P. Günter, ed., *Nonlinear Optical Effects and Materials*, vol. 72 of *Optical Science* (Springer, Berlin, Heidelberg, New York, 2000).
2. M. C. Gupta and J. Ballato, *The Handbook of Photonics* (CRC Press, 2007).
3. H. S. Nalwa, ed., *Organic Electronics and Photonics*, vol. 2 (American Scientific Publishers, 2008).
4. Y. Q. Shi, C. Zhang, H. Zhang, J. H. Bechtel, L. R. Dalton, B. H. Robinson, and W. H. Steier, "Low (sub-1-volt) halfwave voltage polymeric electro-optic modulators achieved by controlling chromophore shape," Science **288**, 119–122 (2000).

#99411 - $15.00 USD Received 25 Jul 2008; revised 12 Sep 2008; accepted 15 Sep 2008; published 22 Sep 2008

5. B. M. A. Rahman, S. Haxha, V. Haxha, and K. T. V. Grattan, "Design optimization of high-speed optical modulators," Act. Pass. Opt. Comp. Comm. Vi **6389**, X3890–X3890 (2006).
6. Y. Enami, C. T. Derose, D. Mathine, C. Loychik, C. Greenlee, R. A. Norwood, T. D. Kim, J. Luo, Y. Tian, A. K. Y. Jen, and N. Peyghambarian, "Hybrid polymer/sol-gel waveguide modulators with exceptionally large electro-optic coefficients," Nat. Photonics **1**, 180–185 (2007).
7. H. Tazawa, Y. H. Kuo, I. Dunayevskiy, J. D. Luo, A. K. Y. Jen, H. R. Fetterman, and W. H. Steier, "Ring resonator-based electrooptic polymer traveling-wave modulator," J. Lightwave Techn. **24**, 3514–3519 (2006).
8. D. Rezzonico, M. Jazbinsek, A. Guarino, O. P. Kwon, and P. Günter, "Electro-optic Charon polymeric microring modulators," Opt. Express **16**, 613–627 (2008).
9. D. Rezzonico, S. J. Kwon, H. Figi, O. P. Kwon, M. Jazbinsek, and P. Günter, "Photochemical stability of nonlinear optical chromophores in polymeric and crystalline materials," J. Chem. Phys. **128**, 124713 (2008).
10. Z. Yang, L. Mutter, M. Stillhart, B. Ruiz, S. Aravazhi, M. Jazbinsek, A. Schneider, V. Gramlich, and P. Günter, "Large-size bulk and thin-film stilbazolium-salt single crystals for nonlinear optics and THz generation," Adv. Funct. Mater. **17**, 2018–2023 (2007).
11. J. Ogawa, S. Okada, Z. Glavcheva, and H. Nakanishi, "Preparation, properties and structures of 1-methyl-4-2-[4-(dimethylamino)phenyl]ethenylpyridinium crystals with various counter anions," J. Cryst. Growth **310**, 836–842 (2008).
12. S. Manetta, M. Ehrensperger, C. Bosshard, and P. Günter, "Organic thin film crystal growth for nonlinear optics: Present methods and exploratory developments," C. R. Phys. **3**, 449–462 (2002).
13. M. Thakur, J. Titus, and A. Mishra, "Single-crystal thin films of organic molecular salt may lead to a new generation of electro-optic devices," Opt. Eng. **42**, 456–458 (2003).
14. S. R. Marder, J. W. Perry, and W. P. Schaefer, "Synthesis of Organic Salts with Large 2^{nd}-Order Optical Nonlinearities," Science **245**(4918), 626–628 (1989).
15. U. Meier, M. Bosch, C. Bosshard, F. Pan, and P. Günter, "Parametric interactions in the organic salt 4-N,N-dimethylamino-4'-N'-methyl-stilbazolium tosylate at telecommunication wavelengths," J. Appl. Phys. **83**, 3486–3489 (1998).
16. F. Pan, G. Knöpfle, C. Bosshard, S. Follonier, R. Spreiter, M. S. Wong, and P. Günter, "Electro-optic properties of the organic salt 4-N,N-dimethylamino-4'-N'-methyl-stilbazolium tosylate," Appl. Phys. Lett. **69**, 13–15 (1996).
17. P. Dittrich, R. Bartlome, G. Montemezzani, and P. Günter, "Femtosecond laser ablation of DAST," Appl. Surf. Sci. **220**, 88–95 (2003).
18. L. Mutter, M. Jazbinsek, M. Zgonik, U. Meier, C. Bosshard, and P. Günter, "Photobleaching and optical properties of organic crystal 4-N,N-dimethylamino-4'-N'-methyl stilbazolium tosylate," J. Appl. Phys. **94**, 1356–1361 (2003).
19. T. Kaino, B. Cai, and K. Takayama, "Fabrication of DAST channel optical waveguides," Adv. Funct. Mater. **12**, 599–603 (2002).
20. W. Geis, R. Sinta, W. Mowers, S. J. Deneault, M. F. Marchant, K. E. Krohn, S. J. Spector, D. R. Calawa, and T. M. Lyszczarz, "Fabrication of crystalline organic waveguides with an exceptionally large electro-optic coefficient," Appl. Phys. Lett. **84**, 3729–3731 (2004).
21. L. Mutter, A. Guarino, M. Jazbinsek, M. Zgonik, P. Günter, and M. Dobeli, "Ion implanted optical waveguides in nonlinear optical organic crystal," Opt. Express **15**, 629–638 (2007).
22. L. Mutter, M. Koechlin, M. Jazbinsek, and P. Günter, "Direct electron beam writing of channel waveguides in nonlinear optical organic crystals," Opt. Express **15**, 16828–16838 (2007).
23. B. Ruiz, M. Jazbinsek, and P. Günter, "Crystal growth of DAST," Cryst. Growth Des. (to be published) (2008).
24. Z. Yang, M. Jazbinsek, B. Ruiz, S. Aravazhi, V. Gramlich, and P. Günter, "Molecular engineering of stilbazolium derivatives for second-order nonlinear optics," Chem. Mater. **19**, 3512–3518 (2007).
25. O. P. Kwon, B. Ruiz, A. Choubey, L. Mutter, A. Schneider, M. Jazbinsek, V. Gramlich, and P. Günter, "Organic nonlinear optical crystals based on configurationally locked polyene for melt growth," Chem. Mater. **18**, 4049–4054 (2006).
26. B. J. Coe, J. A. Harris, I. Asselberghs, K. Wostyn, K. Clays, A. Persoons, B. S. Brunschwig, S. J. Coles, T. Gelbrich, M. E. Light, M. B. Hursthouse, and K. Nakatani, "Quadratic optical nonlinearities of N-methyl and N-aryl pyridinium salts," Adv. Funct. Mater. **13**, 347–357 (2003).
27. O.-P. Kwon, S. J. Kwon, M. Jazbinsek, F. D. J. Brunner, J. I. Seo, C. Hunziker, A. Schneider, H. Yun, Y.-S. Lee, and P. Günter, "Organic Phenolic Configurationally Locked Polyene Single Crystals for Electro-Optic and Terahertz Wave Applications," Adv. Funct. Mater. (to be published) (2008).
28. C. Hunziker, S.-J. Kwon, F. Juvalta, O.-P. Kwon, M. Jazbinsek, and P. Günter, "Configurationally locked, phenolic polyene organic crystal 2-{3-(4-hydroxystyryl)-5,5-dimethylcyclohex-2-enylidene}malononitrile: Linear and nonlinear optical properties," J. Opt. Soc. Am. B **25** (2008).
29. T. Kolev, Z. Glavcheva, D. Yancheva, M. Schurmann, D.-C. Kleb, H. Preut, and P. Bleckmann, "2-3-[2-(4-Hydroxyphenyl)vinyl]-5,5-dimethylcyclohex-2-en-1-ylidenemalononitrile," Acta Crystallogr., Sect. E: Struct. Rep. Online **57**, o561–o562 (2001).
30. T. A. Anhoj, A. M. Jorgensen, D. A. Zauner, and J. Hubner, "The effect of soft bake temperature on the polymerization of SU-8 photoresist," J. Micromech. Microeng. **16**, 1819–1824 (2006).

#99411 - $15.00 USD Received 25 Jul 2008; revised 12 Sep 2008; accepted 15 Sep 2008; published 22 Sep 2008

31. F. Agullo-Lopez, J. M. Cabrera, and F. Aullo-Rueda, *Electrooptics: Penomena, Materials and Applications* (Academic Press Inc., San Diego, 1994).
32. C. Bosshard, K. Sutter, P. Prêtre, J. Hulliger, M. Flörsheimer, P. Kaatz, and P. Günter, *Organic Nonlinear Optical Materials*, vol. 1 of *Advances in Nonlinear Optics* (Gordon and Breach, Amsterdam, 1995).
33. G. Joshi and S. M. Pawde, "Effect of molecular weight on dielectric properties of polyvinyl alcohol films," J. Appl. Polym. Sci. **102**(2), 1014–1016 (2006).

1. Introduction

In recent years, a lot of research effort has been devoted to second-order nonlinear optical organic materials due to their high potential in photonic applications such as active wavelength filters, optical switches, modulators and for THz wave generation [1–3]. The materials investigated can be mainly divided in two classes: guest-host or side chain polymers and organic crystals. Both material classes combine high optical nonlinearities with low dielectric constants, which results in higher optical bandwidth (BW $>$ 100 GHz) and lower driving power compared to standard inorganic materials used in telecommunication, e.g. $LiNbO_3$ that have already reached their BW limit at about 40 GHz [4, 5]. Although polymers are potentially cheap and solution processing is rather simple [4, 6–8], they often suffer from thermal and even more often from photochemical instabilities that lead to device degradation [9]. Organic crystals on the other hand offer superior stability and often higher nonlinearities, however, crystal growth with sufficient optical quality for integrated devices is a challenging task [10–13].

4-dimethylamino-N-methyl-4-stilbazolium tosylate (DAST) is a widely studied organic crystal with high electro-optic coefficients ($r_{111} = 77 \pm 8$ pm/V at 800 nm), large electrical bandwidth and a low dielectric constant ($\varepsilon_1 = 5.2$) [14–16]. Many techniques have been investigated for the fabrication of integrated optic devices in DAST such as femtosecond ablation [17], photobleaching [18, 19], graphoepitaxial growth [20], ion implantation [21], and direct e-beam structuring [22]. Despite these promising results, DAST crystal growth with adequate quality for optical applications remains a challenge and therefore the development of better growth techniques [23] and new molecules with improved crystallization properties is subject of present research [10, 11, 24–26].

Recently a new and promising organic nonlinear optical configurationally locked polyene (CLP) crystal with large macroscopic nonlinearity and high thermal stability was developed [27]. 2-{3-(4-hydroxystyryl)-5,5-dimethylcyclohex-2-enylidene}malononitrile (OH1) features high electro-optic coefficients (75 ± 7 pm/V at 785 nm [28]) similar to the ones observed in DAST and additionally a higher crystal symmetry (orthorhombic with point group *mm*2 [29] instead of monoclinic with point group *m* [14]). It exhibits a wide transparency range from 800 nm to 1400 nm with an absorption coefficient $\alpha < 1$ cm^{-1}, where low loss opto-electronic devices can be fabricated. OH1 features very favorable growth characteristics that allow large-area crystalline thin film growth with single crystalline domains larger than 150 mm^2. In this work we present an optimized technique for structuring integrated photonic devices in OH1 and demonstrate electro-optic (EO) phase modulation in wire waveguides with a high in-device electro-optic figure of merit of $n_3^3 \cdot r_{333} = 1520 \pm 40$ pm/V and 620 ± 50 pm/V at 632.8 and 852 nm, respectively.

2. Waveguide fabrication

2.1. Single-crystalline thin film preparation

OH1 single crystals with good optical quality can be grown from a saturated methanol solution. We have developed a method to grow single crystalline thin films of OH1 with thicknesses from 0.05 to 10 μm directly on amorphous substrates. The details of the growth method will be reported elsewhere. The thickness and single crystal area depend on the substrate used and

#99411 - $15.00 USD Received 25 Jul 2008; revised 12 Sep 2008; accepted 15 Sep 2008; published 22 Sep 2008

the growth conditions. For this work we used standard float glass substrates and chose growth conditions that yielded thin film single crystalline domains larger than 150 mm^2 in size that were $5-10\,\mu$m thick. The crystals grow with their polar axis parallel to the substrate. In order to planarize the upper surface of the thin film, the grown thin film crystals were manually polished to $\lambda/4$ surface quality. This step resulted in a homogenous, planparallel, and high optical quality thin film with a thickness of $3-4\,\mu$m. The adhesion of the crystal to the substrate is very strong, which allows the fabrication of even thinner crystal layers using mechanical polishing.

2.2. Waveguide patterning by optical lithography

We have patterned straight waveguides of various geometries using optical lithography. The process steps are schematically depicted in Fig. 1(a)-(d). Since OH1 is soluble in most organic solvents used in conventional lithography processes, a protection layer on top of the crystal is necessary. A clear and viscous solution (10% w/v) of polyvinyl alcohol (PVA) ($87-89\%$ hydrolyzed with molecular weight $M_w = 31000-50000$) was prepared using distilled water as solvent that does not dissolve OH1. The solution was spin-coated at 2000 rpm forming a 500 nm thick protection layer that is resistant to most organic solvents. Although bulk OH1 crystals remain in a stable crystalline form up to the melting temperature at 212 °C, we have observed that micrometer size thin films on glass tend to transform into an amorphous state induced by eventual scratches from non-perfect polishing at temperatures above 90 °C. In order to avoid this a non-standard lithography process with SU8 as photoresist was used [30]. SU8 2005 was spin-coated at 3000 rpm forming a 4.8 μm thick resist layer. The soft-bake and post-exposure bake temperatures were kept below 65 °C. Figure 2(a) shows the patterned resist on top of the PVA-protected thin film crystal. The waveguides are aligned parallel to the x_2-axis of the crystal. This allows to take full advantage of the electro-optic effect with the largest coefficient r_{333} of OH1 for propagating TE-modes, for which the modal electric field oscillates in the direction of the polar x_3-axis of the crystal in the thin film plane.

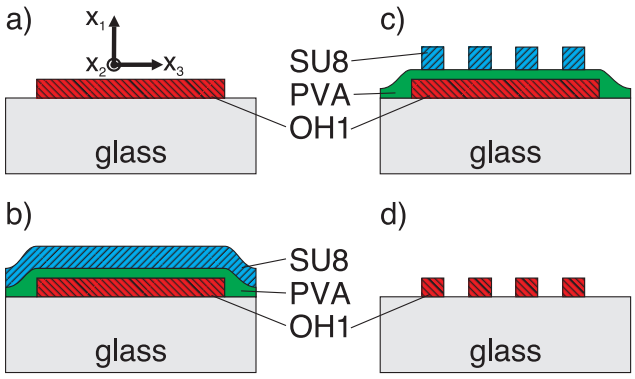

Fig. 1. (a) Orientation of 3-4 μm thick crystalline thin film on glass after solution growth and upper-surface polishing. (b) Deposition of PVA protection layer (480 nm) and SU8 photoresist (4.8 μm). (c) UV-exposure and development of SU8 photoresist. Microscope image in Fig. 2 (a). (d) Optimized pattern transfer by RIE leads to well defined OH1 single-crystalline wires, shown in Fig. 2 (b) from the top and in Fig. 4(a) from the side.

2.3. Pattern transfer by reactive-ion etching

The waveguide pattern was then transferred to the crystal by reactive-ion etching (RIE). Organic materials can be etched with high etch rates using oxygen as reactive agent. Since both, resist

#99411 - $15.00 USD Received 25 Jul 2008; revised 12 Sep 2008; accepted 15 Sep 2008; published 22 Sep 2008

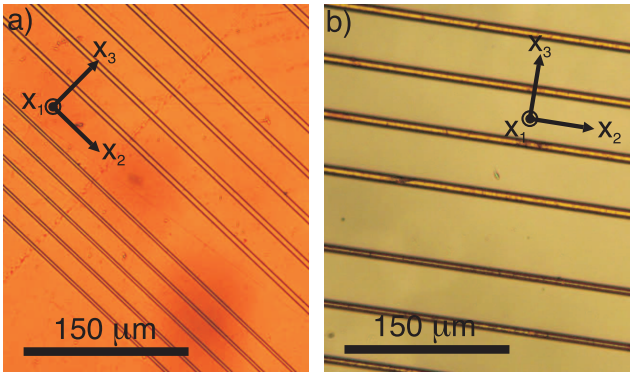

Fig. 2. (a) Microscope image of the developed SU8 photoresist on the protected OH1 single crystalline thin film. (b) Fabricated single crystalline OH1 wires on glass after complete removal of the resist layer by reactive-ion etching.

and crystal are organic compounds it is important to optimize the etch process for OH1, thereby obtaining the best selectivity against SU8. The etch rate of OH1 could be substantially increased by adding CF_4 to the oxygen as etch gas. Figure 3 shows the etch rate of OH1 as a function of the CF_4 concentration. The process was performed on an Oxford Instruments Plasmalab 80 with a total gas flow of 52 sccm for all combinations of gases. For the experimental determination of the etch rates, the chamber pressure was kept at 200 μbar with the rf forward power set to 200 W. The error bars incorporate the measurement uncertainty due to surface inhomogeneities of the unpolished OH1 bulk crystals used for this experiment. The etch rate exhibits a sharp maximum at a gas flow ratio of $CF_4 : O_2 \approx 5 : 21$. At this point an etch rate selectivity of OH1 against SU8 of approximately 1 : 1.35 was obtained. For the pattern transfer of the waveguides into the OH1 crystalline thin film we used a lower chamber pressure of 25 μbar with the same ratio of etch gases. This led to a lower etch rate with the same selectivity between crystal and resist and an improved surface quality of OH1. The etch time was adjusted in order to fully etch away the remaining resist and PVA protection layer on the waveguides. Figure 2 shows a microscope image of a fabricated single crystalline waveguide array after the etch process. We successfully structured waveguides with lateral dimensions of $w = 7.6$, 5.4 and 3.4 μm and a height $h = 3.5$ μm that were 0.8 to 2 mm long.

3. Waveguide characterization

In order to couple light into the waveguides we cleaved the glass substrates perpendicular to the waveguides using a diamond scribe. This produced well defined cross-sectional facets of the waveguides as depicted in Fig. 4(a). Light was coupled into the waveguides by the conventional end-fire coupling technique. The beam diameter of the used laser sources was approximately 1 mm. The coupling lense featured a focal length of 2 mm leading to a beam area in the focal plane of about 10-18 μm^2 in close correspondence with the cross-sectional area of the fabricated waveguides. After propagating through the waveguide, the out-coupled mode was projected onto a CCD camera by means of a microscope objective with a 40$\times$ magnification. A typical modal intensity profile is shown in Fig. 4(b). For the smallest measured waveguides with dimensions of $w \times h = 3.4 \times 3.5$ μm^2 the profiles suggest that only the first order mode can propagate with small guiding losses. Even though simulations show that all three waveguide geometries ($w = 7.6$, 5.4 and 3.4 μm) are not single mode, higher order modes are less strongly confined in the waveguide and therefore, experience higher scattering losses at the sidewalls of

#99411 - $15.00 USD Received 25 Jul 2008; revised 12 Sep 2008; accepted 15 Sep 2008; published 22 Sep 2008

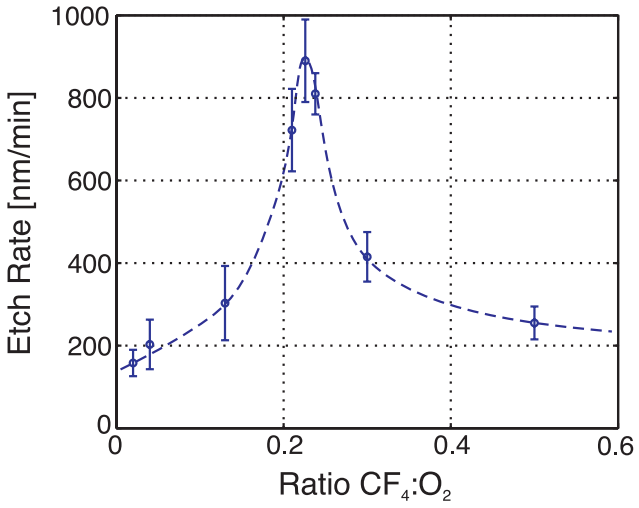

Fig. 3. Etch rate of OH1 at 200 W rf-power as a function of the ratio between CF_4 and O_2 as etch gases. The total gas flow was 52 sccm for all measurements, whereas the chamber pressure was kept at 200 μbar. The dashed curve was added for a better visualization of the experimental data.

the waveguide. The reason for this is a very high index contrast of the produced structures $\Delta n = n_3 - n_{\text{glass}} = 1.16$ and 0.72 at the wavelengths 632.8 nm and 980 nm, respectively. Such high index contrast is very interesting for very large scale integrated (VLSI) photonics, e.g. microring-resonator and photonic crystal devices.

The propagation losses were determined at $\lambda_0 = 632.8$ nm and 980 nm for both, TE- and TM-modes. At $\lambda_0 = 632.8$ nm, close to the absorption edge of OH1 [28], the intrinsic absorption losses in the material are substantial and therefore constitute a dominant contribution to the measured losses. The absorption coefficient, α_2 and α_3 were measured in bulk crystals in [28]. For TE modes the known material absorption α_3 leads to a loss of 46 dB/cm. Assuming $\alpha_1 \approx \alpha_2$ the TM absorption losses can be estimated to be 13 dB/cm. In the range from 800 nm up to 1400 nm light is only very weakly absorbed by OH1 enabling the fabrication of potentially efficient waveguides with losses below 1 dB/cm.

For the determination of the propagation losses, an image of the scattered light was taken from the top of the waveguide using a high resolution infrared sensitive CCD camera (Fig. 4(c)). Assuring the linearity of the detection system, the scattered light is proportional to the guided light intensity $I(z)$ at all positions z along the waveguide, since defect density and roughness can be assumed to be evenly distributed along the waveguide. Under these premises, the propagation loss α can be calculated by analyzing the decrease of the scattered light intensity. For this purpose the intensity profile of the scattered light was summed up along the width of the waveguide to obtain $I(z)$. The resulting exponential decay $I(z) = I_0 \cdot e^{-\alpha z}$ is a measure for the propagation loss α. Figure 5 shows the scattered light intensity as a function of the propagation distance z and illustrates the determination of α for two different waveguide geometries. In Table 1 the smallest measured propagation losses of the fabricated waveguides for different polarizations and geometries $w \times h$ are given. The error specifies the 95% confidence interval of the loss coefficient obtained by least-square analysis of the data. At $\lambda_0 = 980$ nm, propagation losses for TE and TM modes are approximately the same, whereas at $\lambda_0 = 632.8$ nm the losses depend strongly on the polarization due to the large anisotropy of the absorption coefficients [28]. For multimode waveguides at $\lambda_0 = 980$ nm we have obtained losses well

#99411 - $15.00 USD Received 25 Jul 2008; revised 12 Sep 2008; accepted 15 Sep 2008; published 22 Sep 2008

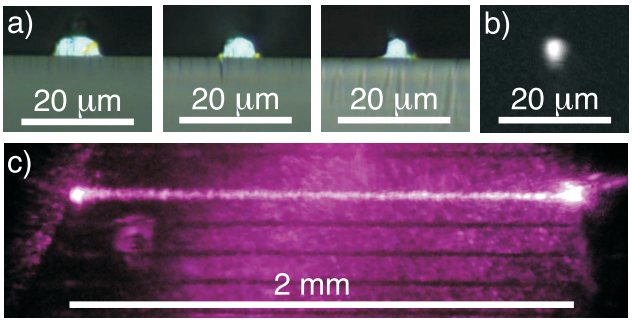

Fig. 4. (a) Cross-sectional profiles of some fabricated waveguides with different width ($w =$ 7.6, 5.4, and 3.4 μm) and height ($h = 3.5$ μm). The pictures were taken with an optical microscope and illumination from the top. (b) Mode profile of a waveguide with dimensions $w \times h = 3.4 \times 3.5$ μm. The out-coupled mode was imaged onto a camera using a 40$\times$ microscope objective. (c) Scattered light in a waveguide imaged with an IR-sensitive CCD camera ($\lambda_0 = 980$ nm).

below 10 dB/cm, which proves that the fabrication method developed is promising for future applications.

Table 1. Propagation losses α for different waveguide geometries $w \times h$ and polarizations. At $\lambda_0 = 632.8$ nm the material absorption alone leads to a loss of 46 dB/cm and 13 dB/cm for TE- and TM-modes, respectively [28].

$w \times h$	$\lambda_0 = 632.8$ nm		$\lambda_0 = 980$ nm
[μm^2]	TE	TM	TE ($\approx$ TM)
7.6×3.5	49 ± 5 dB/cm	16 ± 2 dB/cm	2.1 ± 0.9 dB/cm
5.4×3.5	51 ± 3 dB/cm	20 ± 2 dB/cm	9 ± 1 dB/cm
3.4×3.5	56 ± 3 dB/cm	25 ± 3 dB/cm	17 ± 2 dB/cm

4. Electro-optic phase modulation

The linear electro-optic effect is given by the tensor r_{ijk} which describes the field induced change of the optic indicatrix as [31]

$$\Delta\left(\frac{1}{n^2}\right)_{ij} = \Delta\left(\frac{1}{\varepsilon}\right)_{ij} = r_{ijk}E_k. \tag{1}$$

In crystals with the point group *mm*2 the electro-optic tensor is given by

$$r_{ijk} = r_{mk} = \begin{pmatrix} 0 & 0 & r_{13} \\ 0 & 0 & r_{23} \\ 0 & 0 & r_{33} \\ 0 & r_{42} & 0 \\ r_{51} & 0 & 0 \\ 0 & 0 & 0 \end{pmatrix}, \tag{2}$$

where in OH1 $r_{33} = r_{333} > r_{23} = r_{223}$ are the two largest tensor elements due to the orientation of the charge transfer axes of the molecules in the crystal [28]. An applied modulation voltage V

#99411 - $15.00 USD Received 25 Jul 2008; revised 12 Sep 2008; accepted 15 Sep 2008; published 22 Sep 2008

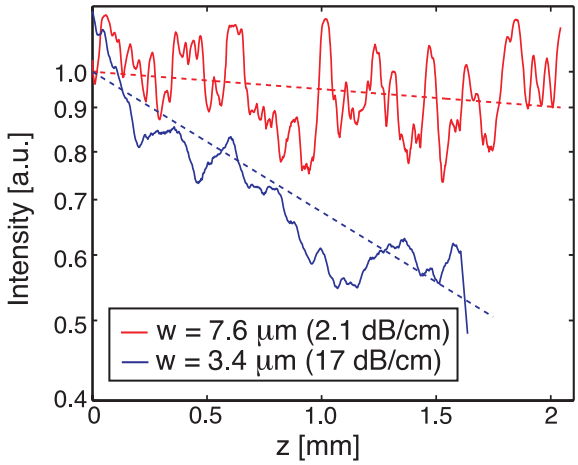

Fig. 5. Scattered light intensity profile on a logarithmic scale along the guiding direction z of two waveguides with different geometry $w \times h$ ($h = 3.5$ μm, $\lambda_0 = 980$ nm).

across a waveguide induces an electric field E in the guiding material which causes a deviation of the refractive index. The guided TE mode experiences therefore a phase shift compared to the case without applied voltage as

$$\Delta\phi = \frac{\pi n_3^3 r_{333} L}{\lambda_0} \cdot E_3 = \frac{\pi}{V_\pi} \cdot V, \tag{3}$$

where n_3 is the refractive index, L is the length of the waveguide and V_π is the half-wave voltage, defined as the voltage required to induce a phase shift $\Delta\phi = \pi$. Eq. (3) is only valid for the case where the effective index of the mode is equal to the refractive index of the guiding material ($n_{\text{eff}} \approx n_3$). For phase-modulation measurements we have used a 1.0 mm long, straight-waveguide sample with cross-sectional dimensions of $w \times h = 3.4 \times 3.5$ μm^2. Gold electrodes have been deposited by vapor deposition using a simple shadow mask. The electrode separation d is 50 μm as shown in Fig. 6. The sample was placed in one arm of a Mach-Zehnder interferometer [32]. A schematic of the setup is shown in Fig. 7. TE-polarized light was coupled into the waveguide with the end-fire coupling technique using a 100$\times$ microscope objective. A sinusoidal modulation voltage with an amplitude $\delta V = 10$ V and a frequency of 1 kHz was applied at the electrodes across the waveguide in the direction of the polar axis of the crystal. The orientation of the polar axis perpendicular to the waveguide leads to a deployment of the largest electro-optic coefficient r_{333} of the OH1 single crystal. The interference pattern with intensity I between the phase-modulated beam and the probe beam in the second arm of the interferometer was converted into an electrical signal using a photodiode. This signal was analyzed with a lock-in amplifier and visualized on an oscilloscope. It can be written as

$$I = I_{\text{m}} + I_{\text{p}} + 2\sqrt{I_{\text{m}} I_{\text{p}}} \cos(\Delta\phi + \phi_0), \tag{4}$$

where I_{m} and I_{p} are the intensities of the modulated and the probe beam, respectively. The electro-optic phase shift (3) is denoted by $\Delta\phi$ and the phase between I_{m} and I_{p} at zero applied voltage across the electrodes ($V = E = 0$) by ϕ_0. In the linear regime where $V \ll V_\pi$, the

#99411 - $15.00 USD Received 25 Jul 2008; revised 12 Sep 2008; accepted 15 Sep 2008; published 22 Sep 2008

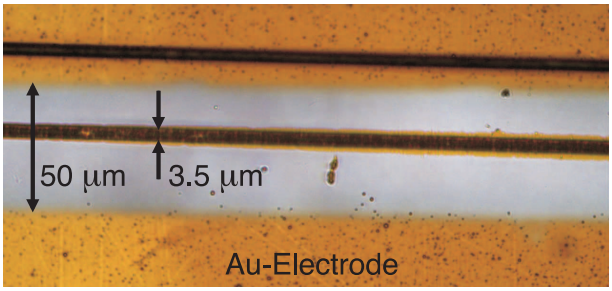

Fig. 6. OH1 waveguide sample used for electro-optic phase modulation. The separation of the gold electrodes is 50 μm.

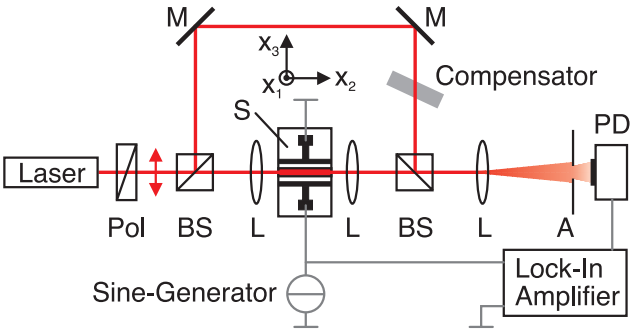

Fig. 7. Setup used for the measurement of electro-optic phase modulation. An interference pattern produced by a phase-modulated beam in the waveguide and a free propagating probe beam is detected by the photodiode. S: waveguide with electrodes, Pol: polarizer, BS: beam splitter, L: lens, M: mirror, A: aperture, PD: photodiode.

modulated intensity δI can be given as a function of the modulation voltage δV by

$$\delta I = \left.\frac{\mathrm{d}I}{\mathrm{d}V}\right|_{V=\Delta\phi=0} \cdot \delta V = -2\sqrt{I_\mathrm{m} I_\mathrm{p}}\sin(\phi_0)\frac{\pi}{V_\pi}\cdot\delta V. \tag{5}$$

A compensator was used to adjust the phase of the probe beam in order to maximize the modulation signal ($\sin(\phi_0) = 1$). It was also used for the determination of the maximum and minimum intensity of the interference I_max and I_min. In these positions, the phase difference in both arms of the interferometer is $\phi_0 = 0$ or π, respectively, and the modulation signal is effectively zero. $\Delta I = I_\mathrm{max} - I_\mathrm{min} = 4\sqrt{I_\mathrm{m} I_\mathrm{p}}$ was typically about 20% of the total signal intensity I, which is due to the different beam shapes of the light in the two arms of the interferometer. The modulation amplitude δI was measured with a lock-in amplifier for better accuracy compared to the oscilloscope. A typical modulation signal as seen on the oscilloscope is shown in Fig. 8 together with the obtained maximum and minimum intensities I_max and I_min. Using (5), a simple expression

#99411 - $15.00 USD Received 25 Jul 2008; revised 12 Sep 2008; accepted 15 Sep 2008; published 22 Sep 2008

for the half-wave voltage in the linear regime ($\sin(\phi_0) = 1, V \ll V_\pi$) can be derived

$$V_\pi = \frac{\pi}{2} \delta V \cdot \frac{\Delta I}{\delta I}. \tag{6}$$

The electric field inside the waveguide with the given electrode configuration shown in Fig. 6

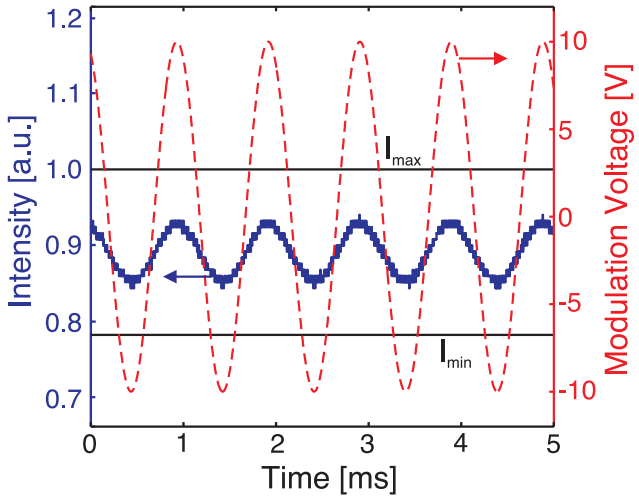

Fig. 8. Electro-optic phase modulation measured in a 1.0 mm long, single-crystalline OH1 waveguide. The applied voltage (dashed) has an amplitude of 10 V and was modulated at a frequency of 1 kHz. The resulting maximized modulation δI of the light intensity (solid) can be extracted from the waveform. $I_{\max}$ and $I_{\min}$ represent the intensities for maximum constructive and destructive interference obtained in the given measurement, respectively.

was calculated with the simulation package Femlab from COMSOL. The electric field in the guiding material is smaller than in the air due to the difference in the dielectric constant ε_r. For the simulation we used $\varepsilon_{r,x_3} = 5.26$ as the dielectric constant along the polar axis of OH1, which is an extrapolated value from THz-frequency range measurements [27]. Fig. 9 shows the calculated electric field in the cross section of the waveguide-electrode system. For the electric field inside the guiding region we obtained $\delta E = 0.05 \pm 0.01$ V/μm at an applied voltage of $\delta V = 10$ V across the electrodes. The error specifies the standard deviation of the field inside the waveguide area. For the determination of the refractive index change as a consequence of the electro-optic effect, the field was considered to be homogenous across the waveguide. The results of the measured half-wave voltage based on (6), the calculated half-wave voltage based on (3), and the calculated average electric field in the waveguide, are given in Table 2. Calculations with mode-solver package Selene from Olympios have shown that the first order TE-mode is very well confined and exhibits an effective index n_{eff} very close to the bulk value of $n_3 = 2.67$ and $n_3 = 2.30$ for the wavelengths of 632.8 and 852 nm, respectively. Therefore, we used the bulk refractive indices ($n_3 \approx n_{\text{eff}}$) for the calculation of the half-wave voltage $V_{\pi,\text{calc}}$ according to (3). In the experiment we have obtained a little more than 70% of the calculated values based on the bulk electro-optic coefficients measured in [28]. This is possibly due to the fact that the measured waveguides were not strictly single-mode and higher order modes with lower effective indices were decreasing the measured effect. The experimental determination of V_π has been repeated with different size waveguide samples, yielding very similar results. The half-wave voltage $\times$ interaction length product $V_\pi \cdot L$ resulting from the current configuration is 8.4 Vcm and 28 Vcm at 632.8 nm and 852 nm, respectively.

#99411 - $15.00 USD Received 25 Jul 2008; revised 12 Sep 2008; accepted 15 Sep 2008; published 22 Sep 2008

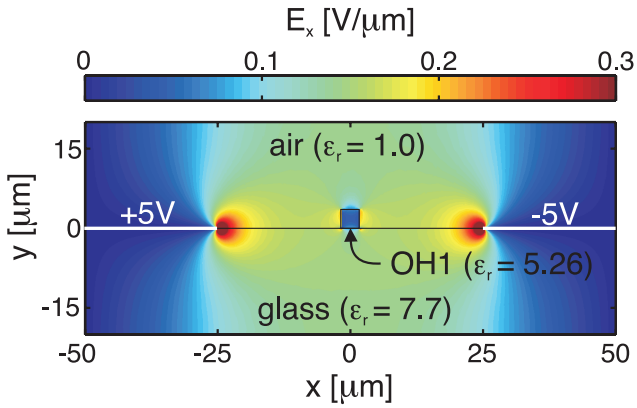

Fig. 9. Electric field distribution in the cross-sectional plane of the fabricated waveguide-electrode system calculated by Femlab. The field inside the waveguide is reduced compared to its surrounding due to the difference in the dielectric constant.

Table 2. Measured $V_{\pi,\mathrm{exp}}$ and calculated $V_{\pi,\mathrm{calc}}$ half-wave voltages in single crystalline waveguides of OH1 at the wavelengths $\lambda_0 = 632.8$ and 852 nm. The calculated values are based on a simulated electric field in the waveguide-electrode system and the bulk electro-optic coefficients $r_{\mathrm{bulk}} = r_{333}(\lambda_0)$ [28].

λ_0 [nm]	r_{bulk} [pm/V]	$V_{\pi,\mathrm{calc}} \cdot L$ [Vcm]	$V_{\pi,\mathrm{exp}} \cdot L$ [Vcm]	exp/calc [%]
632.8	109 ± 4	6.2 ± 0.2	8.4 ± 0.3	74%
852	≈ 71	≈ 20	28 ± 3	72%

The geometry of the electrodes has not been optimized in these first experiments and can be considerably improved by reducing the electrode spacing d. A cladding with a similar dielectric constant as OH1 will further reduce the half-wave voltage of the device. A PVA thin film presents a possible solution since it features a dielectric constant $\varepsilon_{\mathrm{r,PVA}} = 5.08$ at 1 MHz [33] and it is water-soluble and therefore processable in combination with OH1. Calculations using Femlab have shown that a more densely packed electrode configuration with a spacing of 1 μm between waveguide and electrode on both sides increases the average electric field in the guiding material from $\delta E = 0.05 \pm 0.01$ V/μm (our configuration) to $\delta E = 1.1 \pm 0.1$ V/μm at the same applied voltage of $\delta V = 10$ V. The smaller deviation of the electric field from the mean value in the optimized case implies an even more homogenous field compared to the configuration of the experiment. The calculated electric field is shown in Fig. 10. The proposed geometry leads to an increase of the electro-optic efficiency by a factor of more than twenty. Consequently, a reduction of the half-wave voltage $\times$ length product $V_\pi \cdot L$ to 0.29 Vcm and 0.94 Vcm at the wavelengths of 632.8 nm and 852 nm may be achieved, respectively, using the electro-optical coefficients $r_{333} = 109$ pm/V and 71 pm/V measured in the bulk.

5. Conclusion

We have developed a new and promising technique for the fabrication of single crystalline waveguides with very high electro-optic activity based on OH1. Single crystalline OH1 thin films with thicknesses between 5-10 μm have been grown directly on glass substrates. The

#99411 - $15.00 USD Received 25 Jul 2008; revised 12 Sep 2008; accepted 15 Sep 2008; published 22 Sep 2008

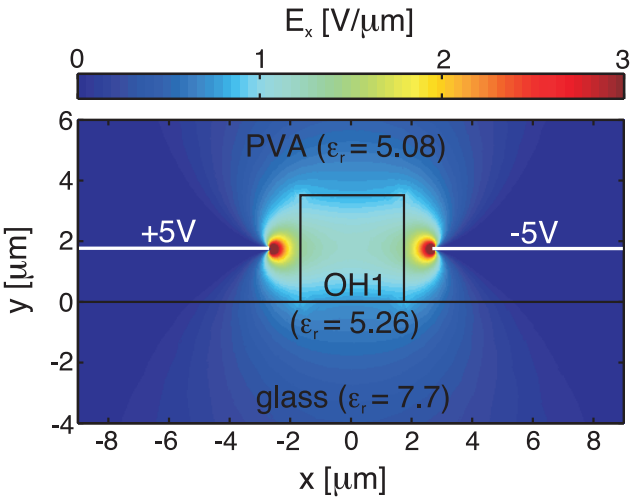

Fig. 10. The calculated electric field in the optimized waveguide-electrode system is homogeneously distributed within the guiding area. The proposed electrode configuration in combination with a PVA waveguide cladding enhances the electro-optic efficiency by a factor of more than 20.

material features high crystal symmetry (*mm*2) and grows with its polar *c*-axis parallel to the thin film surface. We have developed an optimized optical lithography process with SU8 as photoresist to fabricate electro-optic waveguides with dimensions of $3.4 \times 3.5\ \mu\mathrm{m}^2$ and above. The waveguide pattern in the resist was transferred to the crystal using oxygen-RIE with 23% of added CF_4 as reactive agent. This improved the etch rate and optimized the selectivity of the etch process between OH1 and resist. The fabrication of waveguides with high index contrast has shown that the technique is capable of producing low loss waveguides with propagation losses well below 10 dB/cm at $\lambda_0 = 980$ nm for both TE and TM polarization. The high crystal symmetry of OH1 allows a simple orientation of the thin films in order to access the highest electro-optic coefficient r_{333} (109 pm/V at 632.8 nm). This is an important advantage compared to other electro-optic crystals with lower symmetry. We have demonstrated electro-optic phase modulation in the fabricated waveguides featuring half-wave voltages of 8.4 Vcm and 28 Vcm at 632.8 nm and 852 nm, respectively. The excellent performance of the electro-optic phase modulation in straight waveguides with high index contrast proves that this technology is highly promising for future opto-electronic applications, e.g. Mach-Zehnder or microring based modulators or filters. Calculations of the electric field in the guiding material have shown that an optimized electrode configuration can reduce the half-wave voltage $\times$ length product $V_\pi \cdot L$ from 8.4 Vcm and 28 Vcm to 0.29 Vcm and 0.94 Vcm at $\lambda_0 = 632.8$ nm and 852 nm, respectively.

Acknowledgments

We thank J. Hajfler for his expert crystal polishing. Financial support by the Swiss National Science Foundation (SNSF) is gratefully acknowledged.

#99411 - $15.00 USD Received 25 Jul 2008; revised 12 Sep 2008; accepted 15 Sep 2008; published 22 Sep 2008